NASA TECHNICAL
MEMORANDUM

NASA TM X-2075

EFFECT OF RETROROCKET CANT ANGLE ON GROUND EROSION — A SCALED VIKING STUDY

by Leonard V. Clark

Langley Research Center
Hampton, Va. 23365

NATIONAL AERONAUTICS AND SPACE ADMINISTRATION • WASHINGTON, D. C. • OCTOBER 1970

1. Report No. NASA TM X-2075	2. Government Accession No.	3. Recipient's Catalog No.
4. Title and Subtitle EFFECT OF RETROROCKET CANT ANGLE ON GROUND EROSION – A SCALED VIKING STUDY		5. Report Date October 1970
		6. Performing Organization Code
7. Author(s) Leonard V. Clark		8. Performing Organization Report No. L-7376
9. Performing Organization Name and Address NASA Langley Research Center Hampton, Va. 23365		10. Work Unit No. 124-08-29-01
		11. Contract or Grant No.
12. Sponsoring Agency Name and Address National Aeronautics and Space Administration Washington, D.C. 20546		13. Type of Report and Period Covered Technical Memorandum
		14. Sponsoring Agency Code

15. Supplementary Notes

16. Abstract

An experimental study was conducted at the Langley Research Center to evaluate the relative merits of canting the Viking lander retrorockets toward the spacecraft center line as a means of reducing rocket-exhaust disturbance of the surface of Mars. This paper describes the experimental study, outlines the scaling scheme of the tests, and briefly discusses significant data trends. The results of this exploratory study indicate that canting of the retrorockets toward the center of the spacecraft does reduce ground erosion of the landing site from that produced by a lander configuration with downward-directed retrorockets. Obviously, before canting the Viking lander retrorockets, it would be necessary to weigh this reduction in surface disturbance against the attendant loss of thrust due to canting.

17. Key Words (Suggested by Author(s)) Jet impingement Rocket-exhaust effects	18. Distribution Statement Unclassified – Unlimited		
19. Security Classif. (of this report) Unclassified	20. Security Classif. (of this page) Unclassified	21. No. of Pages 24	22. Price* $3.00

EFFECT OF RETROROCKET CANT ANGLE ON GROUND
EROSION – A SCALED VIKING STUDY

By Leonard V. Clark
Langley Research Center

SUMMARY

An experimental study was conducted at the Langley Research Center to evaluate the relative merits of canting the Viking lander retrorockets toward the spacecraft center line as a means of reducing rocket-exhaust disturbance of the surface of Mars. This paper describes the experimental study, outlines the scaling scheme of the tests, and briefly discusses significant data trends. The results of this exploratory study indicate that canting of the retrorockets toward the center of the spacecraft does reduce ground erosion of the landing site from that produced by a lander configuration with downward-directed retrorockets. Obviously, before canting the Viking lander retrorockets, it would be necessary to weigh this reduction in surface disturbance against the attendant loss of thrust due to canting.

INTRODUCTION

Several recent papers have suggested that the area in which the Viking lander space-craft sets down on the surface of Mars may be physically, chemically, and/or biologically altered by the spacecraft's retrorocket exhaust gases. (See refs. 1 to 5.) Since a prime mission objective of such a vehicle is to search for the existence of native Martian life forms, any alteration of the surface in the vicinity of the spacecraft which could compromise the results from specific scientific experiments should be minimized. The three-retrorocket configuration of the Viking lander would cause considerable disturbance to the landing site, particularly in the vicinity of each rocket. One suggested means for possibly reducing the degree of erosion at the periphery of the landing-site area is the use of nozzle canting, whereby the exhausts would be focused toward a single spot beneath the spacecraft. Accordingly, an exploratory experimental study was undertaken to investigate the effects on ground erosion of canting of the retrorockets toward the center of the spacecraft. The study was conducted in the Langley 60-foot vacuum sphere over a range of ambient pressures which bracket the expected Martian conditions and involved the firing of cold-gas jets which descended at a constant velocity toward a particulate target

surface. This paper describes the experimental study, outlines the scaling scheme of the tests, and briefly discusses significant data trends.

SYMBOLS

a   speed of sound in gas

C_f aerodynamic friction coefficient on exposed particle

c   particle packing factor

d   diameter

F   thrust of a single rocket

g   gravity

h   height above target surface as measured to nozzle-exit plane

l length

M   Mach number

m   mass

N_{Fr} Froude number

p   pressure

R   gas constant

T   temperature (absolute)

t   time

V   volume

v   velocity

y	crater depth
α	particle friction angle
β	rocket cant angle
γ	ratio of specific heats of gas
ϵ	expansion ratio
θ	nozzle expansion half-angle
λ	ratio of aerodynamic shear force to particle frictional restraint force
ρ	density
$\doteq$	dimensional equivalence

Subscripts:

c	nozzle combustion chamber
e	nozzle exit
F	full scale
g	gas
M	model
s	surface
∞	ambient (60-foot vacuum sphere)
1,2,3	refers to cold-gas jets

A bar over a symbol denotes an average value.

APPARATUS

General Setup

The present experimental investigation was conducted in the Langley 60-foot vacuum sphere, which is shown in the photograph of figure 1. The test apparatus for the Mars landing-site alteration study is shown in the schematic of figure 2 and in the photograph of figure 3. The model Viking lander was cantilevered from a carriage which was free to move along a vertical rail which extended from the top of the vacuum chamber to the floor of the chamber and was alined perpendicular to the target surface. The model Viking lander, moved by an electric-motor-driven chain-and-brake system, was positioned so that the exhausts from its three cold-gas jets would impinge during descent upon a particulate target surface.
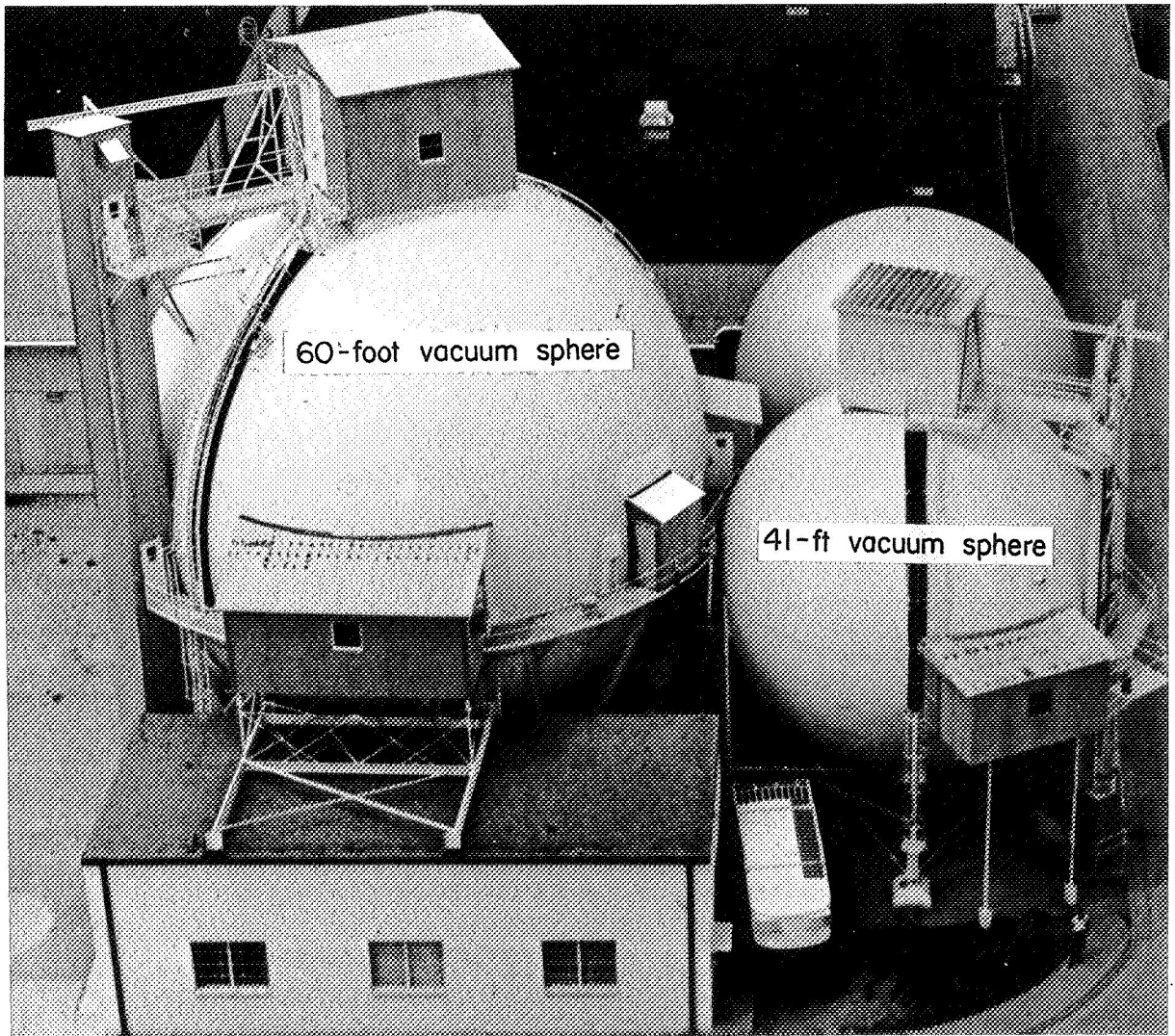
L-64-7831.1

Figure 1.- Photograph of large vacuum chambers at Langley Research Center.

Model Viking Lander

The Viking lander was represented during the experimental tests by a triangular plate with a jet mounted at each apex. The model spacecraft, shown schematically in figure 4, was configured so that each jet could be directed at a selected angle toward the spacecraft center line by rotation about an axis which passed through the nozzle throat. The lander retrorockets were simulated by nozzles designed for use with helium.

Part of the planned sequence of events leading to Mars landing and a tentative representation of the Viking lander spacecraft are depicted in figures 5 and 6, respectively. For the purposes of the present study, the important part of the landing sequence is the retrorocket firing, which commences at an altitude of 1463 meters (8940 rocket-exit diameters) above the surface of Mars. The lander continues to follow a gravity-turn trajectory to an altitude of 15 meters ($100d_e$), whereupon the terminal descent retrorockets are throttled and the lander descends at constant velocity (approximately 3 m/s) to an altitude of 3 meters ($20d_e$). Retrothrust is then terminated, and the lander falls to the Mars surface; the three-legged landing gear of the lander absorbs the remaining energy.
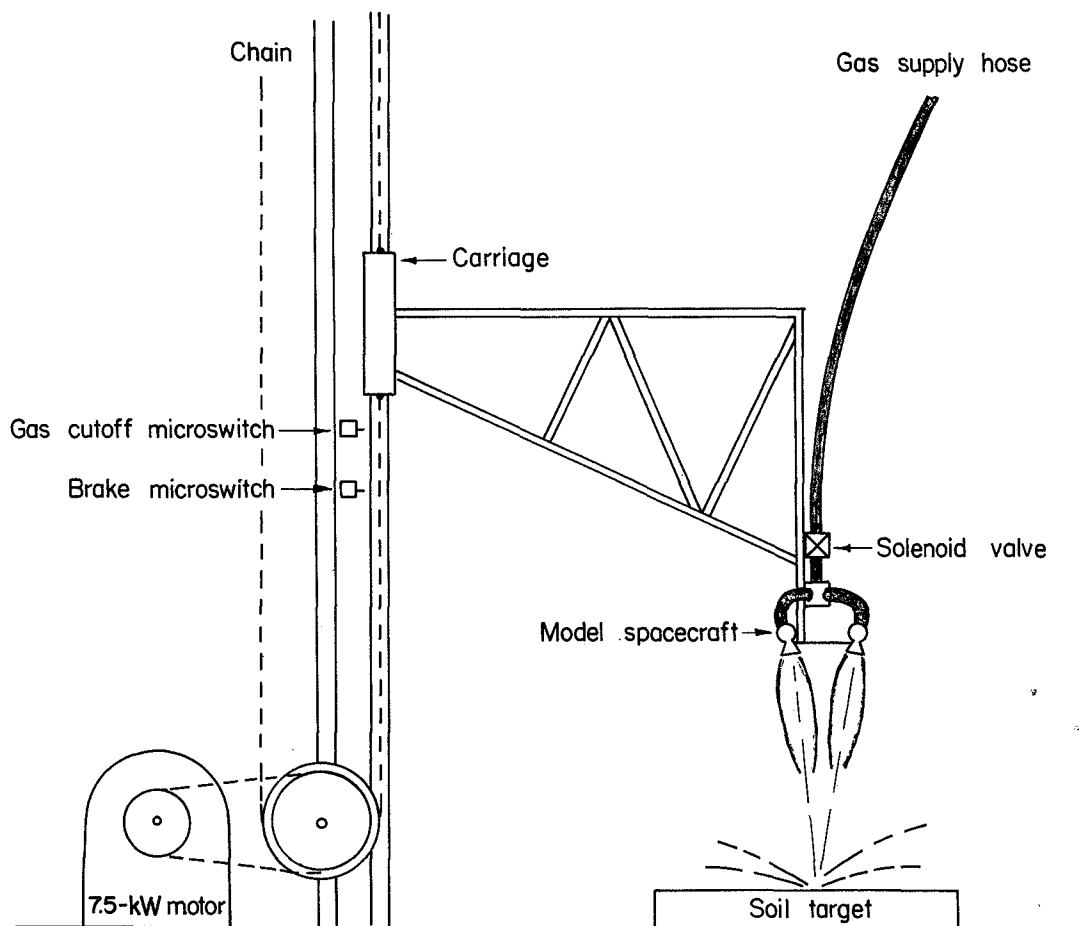

Figure 2.- Schematic of test apparatus.

Gas supply hose

Solenoid valve

Base pressure gage

Chamber pressure gage

Nozzles

Target surface
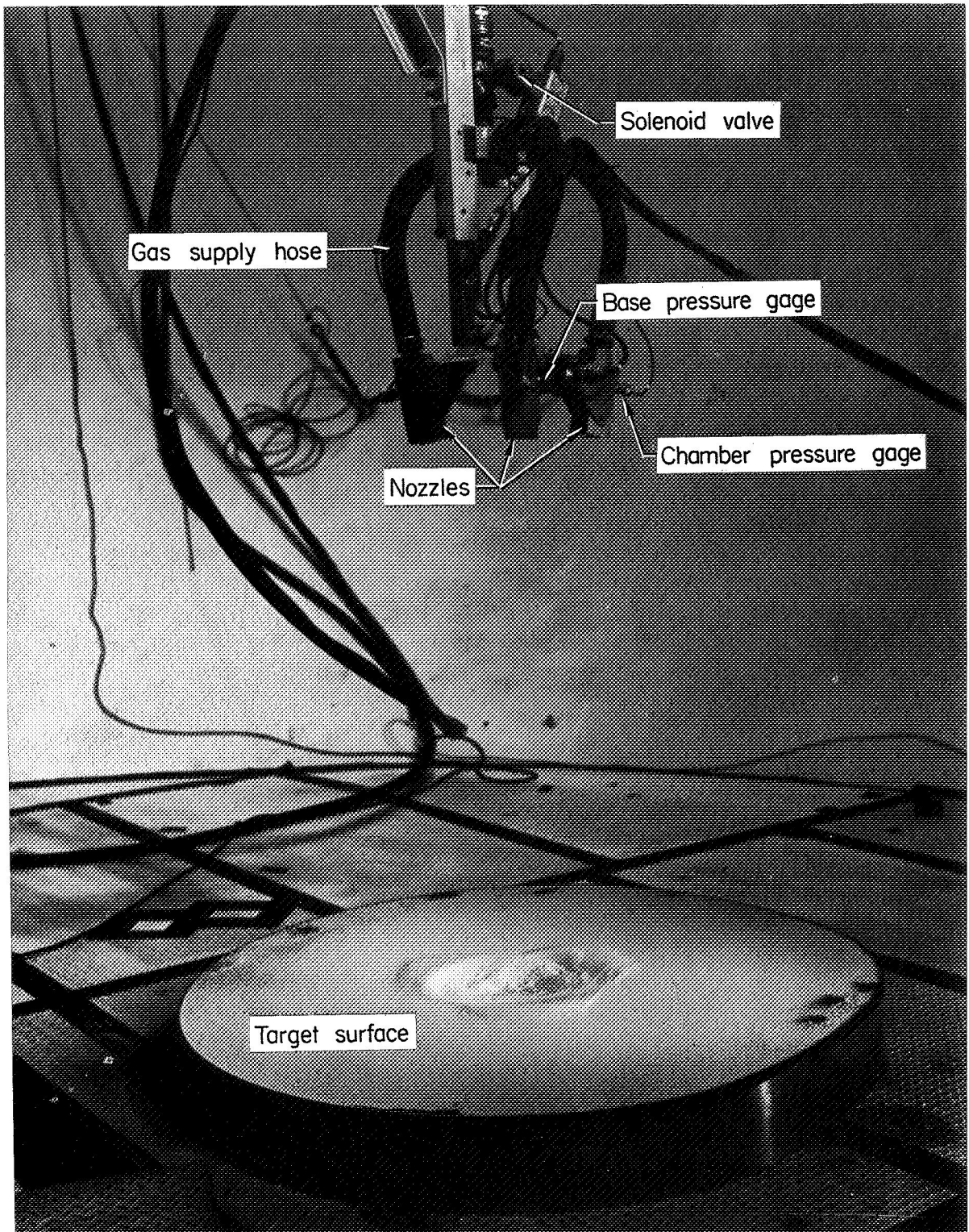
L-70-2031.1

Figure 3.- Photograph of test apparatus installed in Langley 60-foot vacuum sphere.

To simplify testing and because the descent trajectory of the Viking lander has not been precisely defined, a constant-velocity vertical descent was selected for the model spacecraft.

Target

The target surface during the tests was a bed of solid glass beads each having a nominal diameter of 0.15 mm. The density of the solid glass is 2.5 g/cm^3; whereas the bulk density of these beads in the target container is estimated at 1.5 g/cm^3. The center line of the model spacecraft was alined to pass through the center of the test bed, which
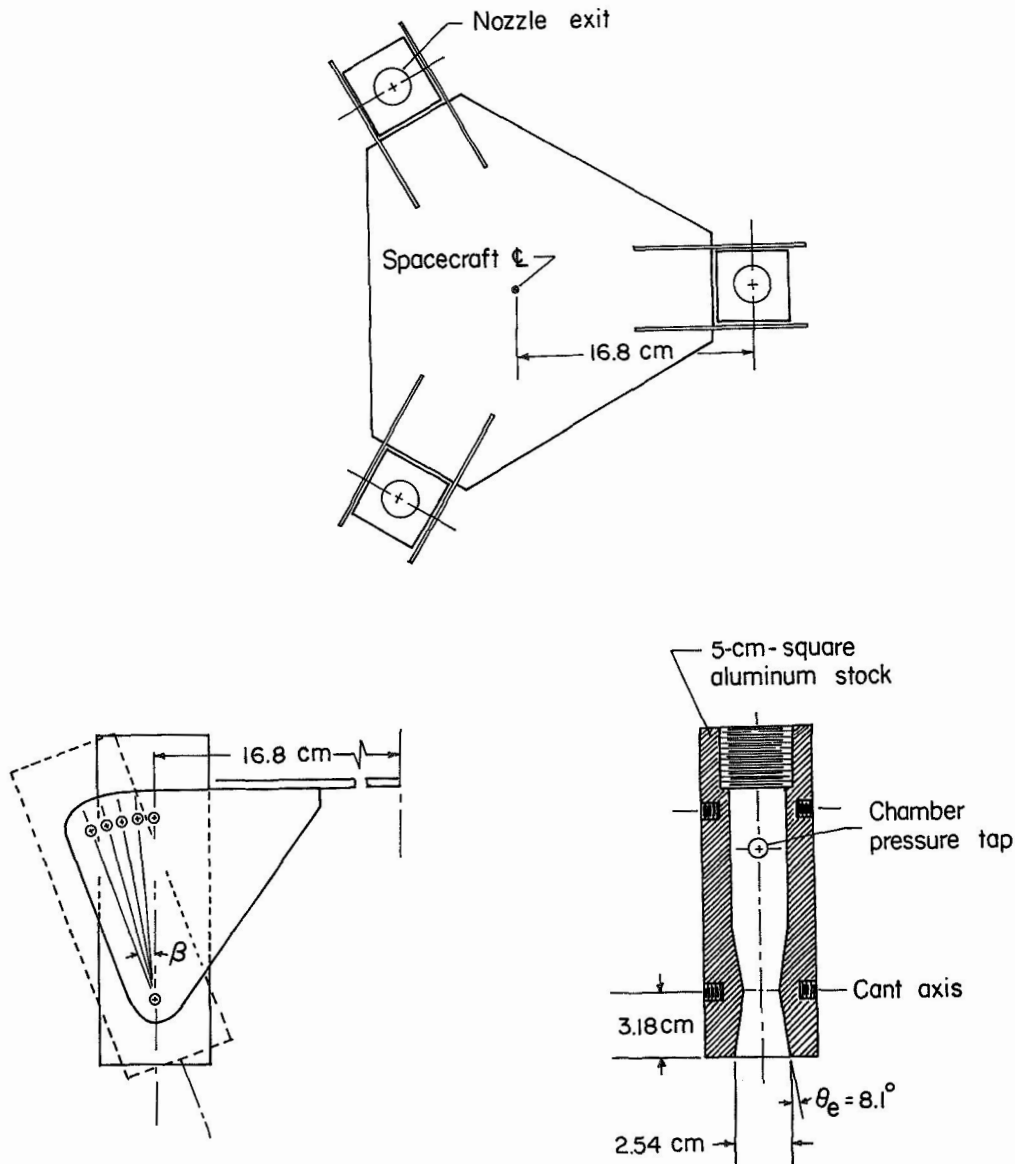

Figure 4.- Schematic of model spacecraft.

was 1.2 meters in diameter and 15 cm deep. In order to minimize any interference of the jet exhausts with the support structure, the test bed was centered 1.8 meters from the vertical rail along which the mounting carriage for the model spacecraft moved.

Instrumentation

The "combustion-chamber" pressure was measured in each of the three nozzles with a 100-kN/m^2-capacity strain-gage-type pressure gage. In addition, one of the nozzles was instrumented to measure combustion-chamber temperature. The descent velocity of the model spacecraft was determined from a potentiometer attached to the drive-chain gear. For some of the tests, a 3.5-kN/m^2-capacity pressure gage was mounted between the nozzles on the center line of the spacecraft to measure possible exhaust-gas pressure on the base of the vehicle during surface approach caused by either interacting exhausts or surface-reflected exhaust gases. The outputs from all of the various gages were recorded on a direct-write oscillograph recorder for subsequent data reduction.

Entry

Parachute deployed (M ≤ 2, h = 5486 m)

Aeroshell separates (M ≤ 0.8, h = 4267 m)

Initiate terminal engines (h = 1463 m)

Separate parachute base cover
(v ≤ 100 m/s, h = 1189 m)

Begin constant velocity descent
(v = 3 m/s, h = 15 m)

Touchdown
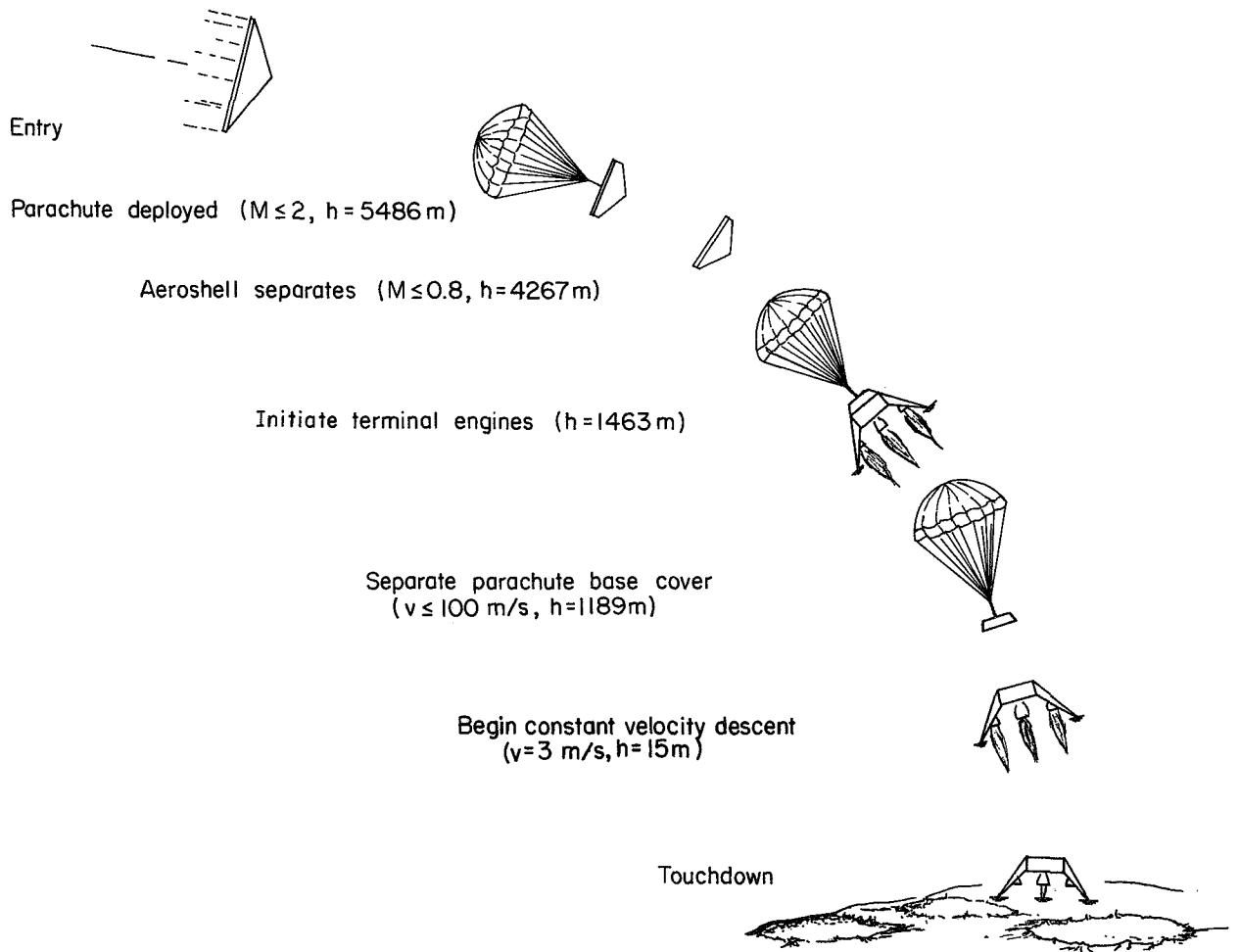
Figure 5.- Proposed Mars landing sequence.

The target surface was filmed during the tests by use of a high-speed camera located inside the vacuum chamber. The camera, which was contained in a box vented to atmospheric pressure, was operated at a nominal speed of 400 frames per second. Timing marks applied to one edge of the film permitted the model-spacecraft altitude at the onset of surface erosion to be determined by detailed analysis of the film on a motion analyzer.

TEST PROCEDURE

The test procedure consisted of initially evacuating the 60-foot vacuum sphere to the desired level of ambient pressure. Before each test the thrust level of the jets was checked by a 0.5-second firing with the model spacecraft at the top of the chamber (in order not to disturb the target surface). Adjustments to the nozzle combustion-chamber pressures were made as required to regulate their thrust level with a manually operated valve located at the high-pressure helium source (a bottle farm located outside the vacuum chamber). The model retrorockets were then fired, and the spacecraft was lowered at constant velocity toward the target surface. Microswitches located along the vertical rail were tripped by the passage of the carriage from which the model spacecraft was cantilevered. A gas cutoff microswitch terminated nozzle thrust at selected spacecraft altitudes above the surface. A brake microswitch reversed the descent-control motor
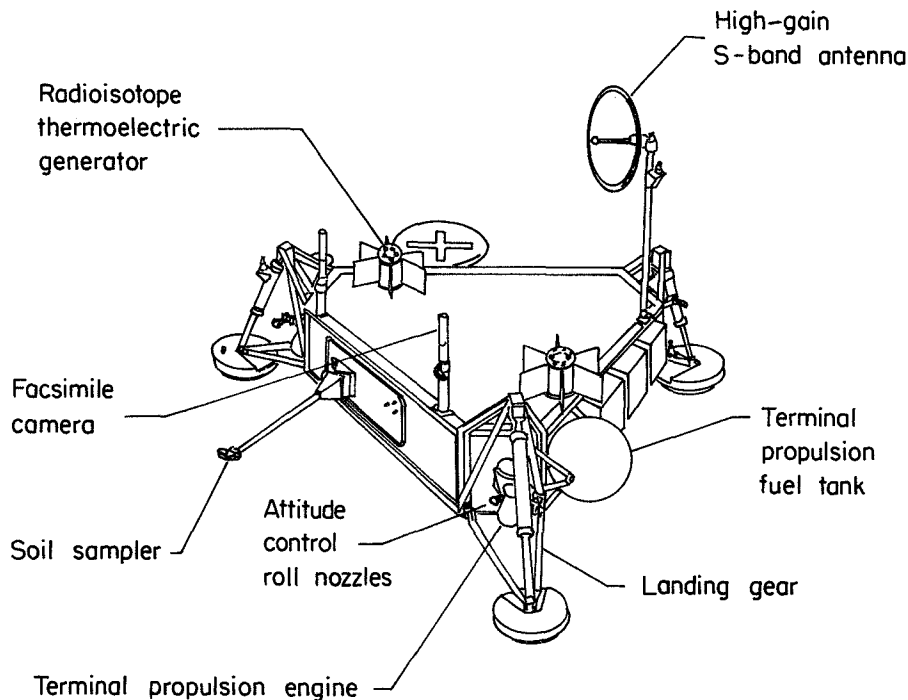

Figure 6.- Proposed Viking lander configuration.

to slow the spacecraft before the model impacted the target surface. Thrust tailoff times during the present tests averaged 0.035 second.

After the chamber was slowly vented to earth atmosphere, the target surface disturbance was photographed and measured. The target bed was subsequently refilled and smoothed for the next test. For most of the tests, the predominantly white target surface was then sprayed lightly with black paint in order to improve conditions for observing the exhaust-surface interaction. Also, the onset of erosion could be determined with greater precision by observing the target surface as the top layer of black particles eroded to reveal white particles.

<div align="center">SCALING CONSIDERATIONS</div>

The present tests were conducted with an experimental setup intended to be representative of the Viking lander during a soft landing on Mars. The general effect of rocket cant angle on the surface erosion pattern should be the same in laboratory tests as on Mars if the model rocket exhausts are expanded similarly to the full-scale rocket exhausts (to provide the same relative interference between exhausts). The model rocket conditions were therefore chosen to provide similar-shaped plumes as full scale at ambient pressures which bracket the expected Martian conditions. For a quantitative interpretation of the model results, the succeeding paragraphs describe the scaling approach that was followed for the present tests.

From practical considerations (e.g., wanting to simulate high spacecraft altitudes in the vacuum chamber and to avoid exhaust condensation) the length scale of the model was chosen to be 1/6 of the planned full-scale dimension, and helium was chosen as the model gas. A rocket-exhaust energy distribution parameter $\gamma(\gamma - 1)M_e^2$ was chosen as the principal scaling parameter. This parameter is proportional to the ratio of exhaust-gas kinetic energy to exhaust-gas internal energy. (See ref. 6.) Maintaining this parameter insures the proper energy distribution in the model exhaust and establishes the time scale.

$$\gamma_M\left(\gamma_M - 1\right)M_M^2 = \gamma_F\left(\gamma_F - 1\right)M_F^2 \tag{1}$$

where

$$M^2 = \left(\frac{v}{a}\right)^2 = \frac{v^2}{\gamma RT} \doteq \frac{(l/t)^2}{\gamma RT} \tag{2}$$

Substituting for M^2 in equation (1) and solving for the time scale ratio gives

$$\frac{t_F}{t_M} = \frac{l_F}{l_M}\left[\frac{R_M T_M\left(\gamma_F - 1\right)}{R_F T_F\left(\gamma_M - 1\right)}\right]^{1/2} \tag{3}$$

10

Evaluating the time scale ratio by using rocket-exit values from table 1 for model and full-scale properties yields

$$\frac{t_F}{t_M} = 3.9 \tag{4}$$

The mass scale ratio may be determined from the equation

$$\frac{m_F}{m_M} = \frac{\rho_F}{\rho_M}\left(\frac{l_F}{l_M}\right)^3 \tag{5}$$

Evaluating the mass scale ratio by using rocket-exit values for gas mass density and the previously chosen length scale ratio yields

$$\frac{m_F}{m_M} = 100 \tag{6}$$

After these fundamental scale ratios for length, mass, and time are determined, other important scale ratios (full scale to model) can be derived:

Velocity scale ratio

$$\frac{l_F}{l_M}\frac{t_M}{t_F} = 1.5$$

Force scale ratio

$$\frac{m_F}{m_M}\frac{l_F}{l_M}\frac{t_M^2}{t_F^2} = 39$$

$\left.\begin{array}{c} \\ \\ \\ \\ \\ \\ \\ \end{array}\right\}$ (7)

The required area ratio of the model retrorocket nozzles was determined from a solution of equation (1); for convenience, a conical shape was chosen for these nozzles. A very low value of model rocket chamber pressure was required in order for the nozzle-exit pressure to equal that for full scale. Since the objective of the tests was to utilize surface disturbance to ascertain the effects of rocket cant angle, the disturbances were amplified by conducting the tests with higher chamber pressure. Consequently, the model tests simulate full-scale conditions for a Mars ambient pressure of about one-half that of each test.

Since the model was scaled only on the basis of the rocket conditions, it is of interest to examine factors concerning the exhaust interaction with particulate surfaces. Soil erosion occurs because of a momentum transfer from the rocket exhaust gas stream to the surface particles. Therefore, a requirement for proper simulation might logically be that the ratios of gas mass density to surface-material mass density be the same for model and full-scale conditions. The density of the surface material of Mars has been estimated to be approximately 3.0 g/cm^3. By substituting numerical values, these density ratios are

$$\left.\begin{array}{l} \dfrac{\rho_{g,F}}{\rho_{s,F}} = 2.9 \times 10^{-6} \\[2em] \dfrac{\rho_{g,M}}{\rho_{s,M}} = 7.3 \times 10^{-6} \end{array}\right\} \tag{8}$$

Therefore for the model, the gas was heavier relative to the particle material than for the assumed full-scale vehicle. Another parameter which should also be examined is the ratio of aerodynamic shear force to particle frictional restraint force. This ratio may be written as

$$\lambda = \frac{C_f \rho_g v^2}{\rho_s g dc \tan \alpha} \tag{9}$$

Evaluating this ratio for the model and full-scale situations (by assuming that C_f, c, and α are the same for the full-scale spacecraft and the model) reveals that for the present tests

$$\frac{\lambda_M}{\lambda_F} = 2.5 \tag{10}$$

Therefore, the model target surface should exhibit considerably more erosion than full scale if everything else is properly scaled, that is, rocket thrust, descent velocity of the lander, and so forth. It is apparent that a Froude number v^2/dg is contained in this parameter. If this is independently maintained, the ratio of particle inertia forces to particle gravity forces would be the same for model and full scale, and the trajectories of full-scale and model particles would be similar. Evaluating the ratio of model and full-scale Froude numbers gives

$$\frac{N_{Fr,M}}{N_{Fr,F}} = 1.0 \tag{11}$$

Therefore, the model particles should travel the same relative distance as the full-scale particles.

RESULTS AND DISCUSSION

Test conditions and measured results of the present experimental study are summarized in tables 2 and 3. Wherever possible, the volume of eroded target surface material was estimated by assuming that the erosion craters could be approximated by spherical segments. In terms of the measured crater characteristics, the equation for computing the volume of a spherical segment is

$$V = \frac{1}{6}\pi y\left(\frac{3d^2}{4} + y^2\right) \tag{12}$$

where y and d are the crater depth and diameter, respectively.

### Effect of Retrorocket Cant Angle

The effect of retrorocket cant angle on landing-site disturbance may be seen in figure 7, which shows photographs of test results at different rocket cant angles for similar test conditions. Comparison of the photographs reveals that the site disturbance pattern changes from three distinct craters (one beneath each rocket) for the rockets directed straight down (0° cant angle) to a single crater centered beneath the spacecraft for the rockets angled toward the center line of the model spacecraft. The dimensions of the craters and the corresponding eroded volumes (table 3) indicate that substantially less material was eroded during tests with the rocket nozzles canted, except for test 6 (shown in fig. 7(b)). For this test the nozzle thrust was 19 percent higher than that for test 5, which possibly accounts for the volume of eroded material being nearly equal for those two tests. It should be noted, however, that the rocket exhausts should be more concentrated for the tests at an ambient pressure of 0.8 kN/m^2, which may also have contributed to the relatively large crater of test 6.

The lateral dimensions of two of the disturbances are superposed in figure 8 to give an indication of their sizes relative to the model spacecraft. The computed erosion crater volumes for these particular tests indicate that 41 percent less material was eroded for the 20° cant-angle test than for the 0° cant-angle test. Perhaps of equal importance, however, is that the craters which result from using uncanted retrorockets may prove to be a landing hazard considering the tentative placement of the spacecraft landing gear in the vicinity of the retrorockets. Prior to canting the Viking lander retrorockets, it would of course be necessary to weigh the advantages against the attendant loss of thrust due to canting ($\cos 5^O = 0.996$, $\cos 10^O = 0.985$, $\cos 15^O = 0.966$, and $\cos 20^O = 0.940$).

Effect of Thrust-Cutoff Altitude

The effect of thrust-cutoff altitude on landing-site disturbance for different rocket cant angles may be seen from the photographs of figure 9. For all the tests, the surface disturbance increased as the rockets came closer to the surface before thrust cutoff. The tests shown in figure 9 correspond to full-scale thrust-cutoff altitudes of 3.4 and 5.8 meters.

Test 2 conditions	
β	0°
$p_{c,1}$	73.6 to 63.4 kN/m^2
$p_{c,2}$	72.7 to 64.6 kN/m^2
$p_{c,3}$	71.9 to 61.0 kN/m^2
p_∞	0.4 kN/m^2
h/d_e	523 to 21.8
$\overline{v}$	2.61 m/s
$\overline{p}_e/p_\infty$	10.3
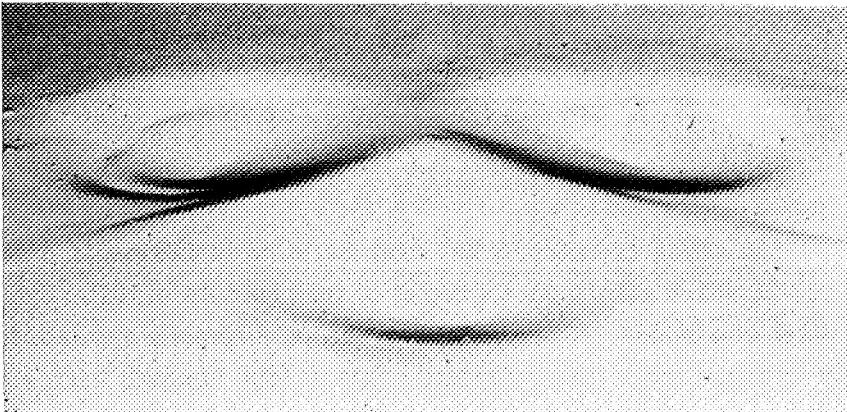
$\beta = 0^\circ$ · L-70-1926

Test 3 conditions	
β	10°
$p_{c,1}$	65.5 to 57.4 kN/m^2
$p_{c,2}$	65.0 to 57.9 kN/m^2
$p_{c,3}$	62.1 to 55.0 kN/m^2
p_∞	0.4 kN/m^2
h/d_e	525 to 21.8
$\overline{v}$	2.69 m/s
$\overline{p}_e/p_\infty$	9.2
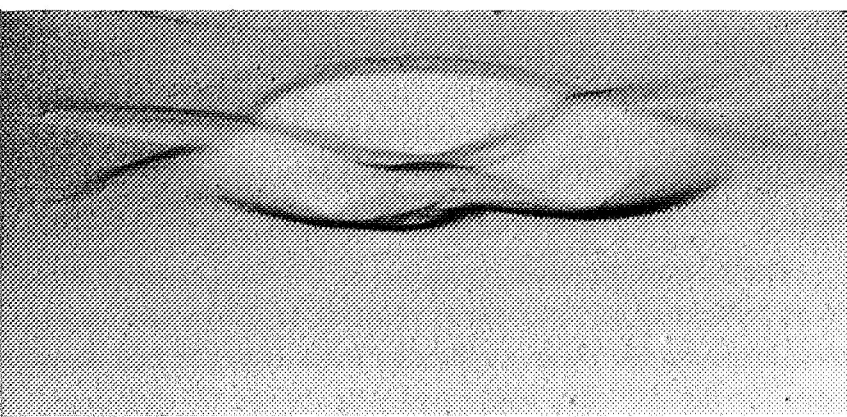
$\beta = 10^\circ$ · L-70-1941

Test 4 conditions	
β	20°
$p_{c,1}$	68.7 to 59.3 kN/m^2
$p_{c,2}$	67.3 to 58.5 kN/m^2
$p_{c,3}$	64.1 to 56.3 kN/m^2
p_∞	0.4 kN/m^2
h/d_e	528 to 21.9
$\overline{v}$	2.60 m/s
$\overline{p}_e/p_\infty$	9.2
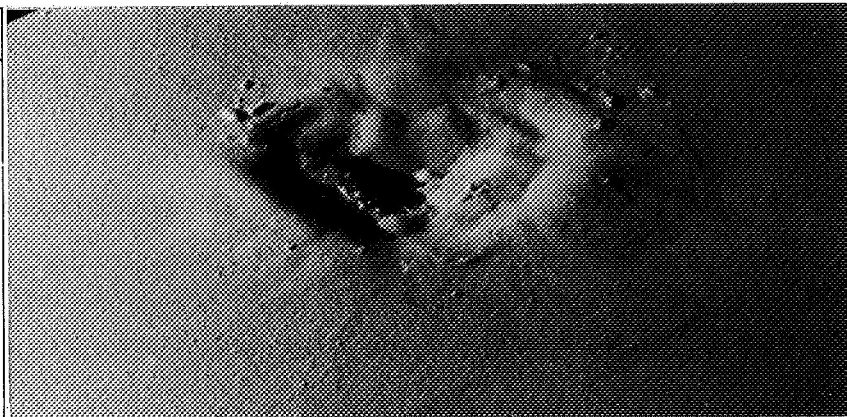
$\beta = 20^\circ$ · L-70-1938

(a) $p_\infty = 0.4$ kN/m^2; $v \approx 2.6$ m/s.

Figure 7.- Test photographs illustrating effect of retrorocket cant angle
on target surface disturbance.

Test 5 conditions	
β	0°
$p_{c,1}$	61.3 to 58.4 kN/m^2
$p_{c,2}$	62.5 to 57.4 kN/m^2
$p_{c,3}$	63.3 to 55.2 kN/m^2
p_{∞}	0.8 kN/m^2
h/d_e	539 to 21.1
$\bar{v}$	2.62 m/s
$\bar{p}_e/p_{\infty}$	4.5

$\beta = 0^{\circ}$ 　　　　　 L-70-1949

Test 6 conditions	
β	15°
$p_{c,1}$	76.1 to 68.9 kN/m^2
$p_{c,2}$	75.4 to 69.3 kN/m^2
$p_{c,3}$	70.8 to 65.8 kN/m^2
p_{∞}	0.8 kN/m^2
h/d_e	535 to 20.9
$\bar{v}$	2.61 m/s
$\bar{p}_e/p_{\infty}$	5.4

$\beta = 15^{\circ}$ 　　　　　 L-70-1960

(b)　$p_{\infty} = 0.8$ kN/m^2;　$v \approx 2.6$ m/s.

Figure 7.- Continued.

Test 7 conditions	
β	0°
$p_{c,1}$	66.7 to 54.7 kN/m^2
$p_{c,2}$	66.8 to 55.4 kN/m^2
$p_{c,3}$	61.7 to 50.9 kN/m^2
p_∞	0.8 kN/m^2
h/d_e	527 to 22.9
$\bar{v}$	1.30 m/s
$\bar{p}_e/p_\infty$	4.5

$\beta = 0^\circ$ L-70-1969

Test 8 conditions	
β	10°
$p_{c,1}$	64.5 to 52.5 kN/m^2
$p_{c,2}$	63.8 to 52.4 kN/m^2
$p_{c,3}$	60.6 to 49.6 kN/m^2
p_∞	0.8 kN/m^2
h/d_e	530 to 22.9
$\bar{v}$	1.29 m/s
$\bar{p}_e/p_\infty$	4.3

$\beta = 10^\circ$ L-70-2001

(c) $p_\infty = 0.8$ kN/m^2; $v \approx 1.3$ m/s.

Figure 7.- Concluded.

Test	p_∞, kN/m^2	β, deg	h/d$_e$	$\bar{v}$, m/s	$\bar{p}_e/p_\infty$	$\bar{F}_M$, N	V, cm^3
2	0.4	0	523 to 21.8	2.61	10.3	23.6	2950
4	.4	20	528 to 21.9	2.60	9.2	21.6	1740

Projection of rocket ℄'s
on surface for h/d$_e$=21.9
and β=20°

Test 2 crater

Test 4 crater

Spacecraft planform

Foot pad
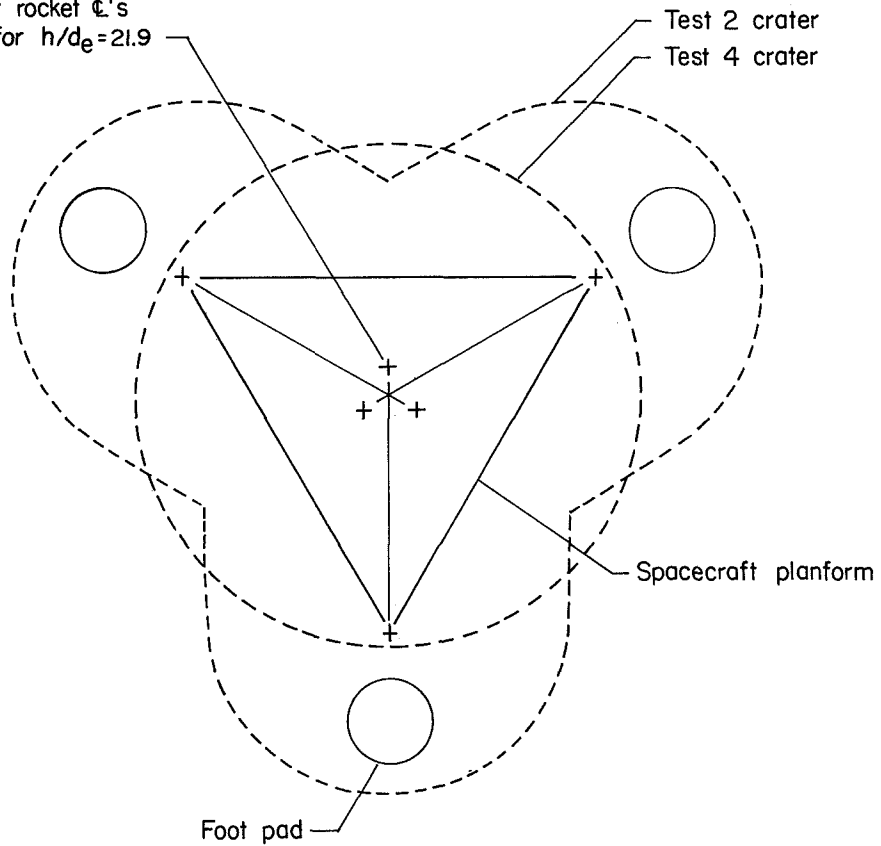
Figure 8.- Superposition of surface disturbances illustrating
effect of retrorocket cant angle.

Test 9 conditions	
β	10°
$p_{c,1}$	63.7 to 55.0 kN/m2
$p_{c,2}$	62.5 to 54.4 kN/m2
$p_{c,3}$	59.9 to 52.5 kN/m2
p_{∞}	0.4 kN/m2
h/d_e	534 to 38.6
$\bar{v}$	2.57 m/s
$\bar{p}_e/p_{\infty}$	8.8
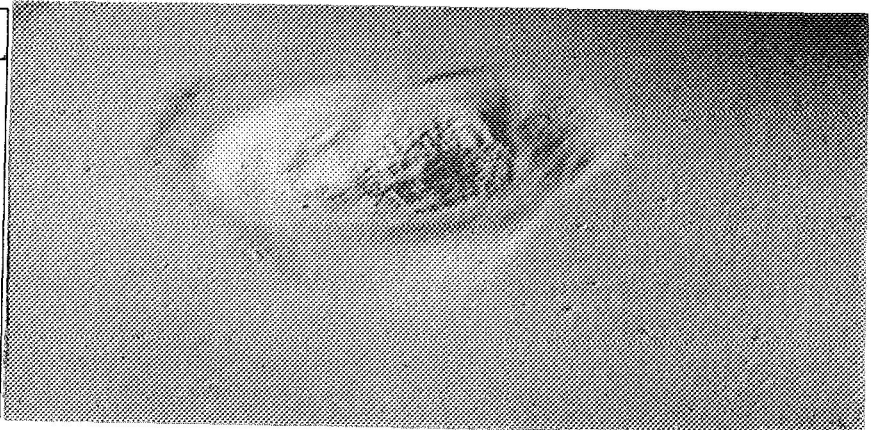
h/d_e = 534 to 38.6   L-70-2030

| Test 3 conditions	
β	10°
$p_{c,1}$	65.5 to 57.4 kN/m2
$p_{c,2}$	65.0 to 57.9 kN/m2
$p_{c,3}$	62.1 to 55.0 kN/m2
p_{∞}	0.4 kN/m2
h/d_e	525 to 21.8
$\bar{v}$	2.69 m/s
$\bar{p}_e/p_{\infty}$	9.2
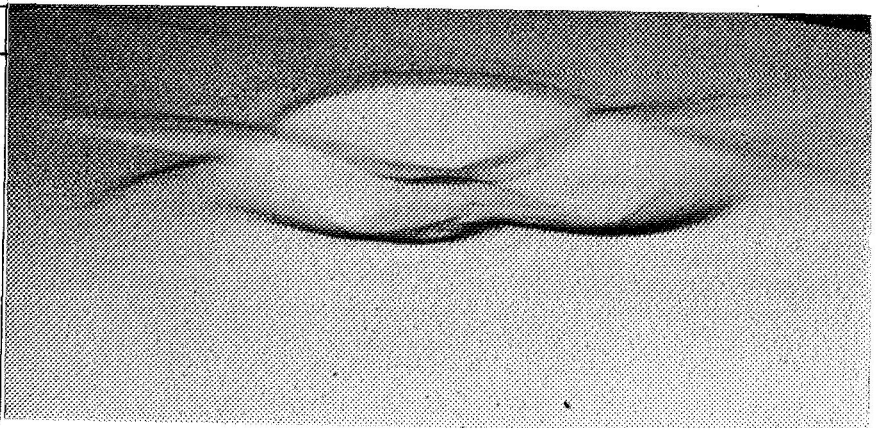
h/d_e = 525 to 21.8   L-70-1941

(a) $\beta = 10^{\circ}$.

Figure 9.— Test photographs illustrating effect of thrust-cutoff altitude
on target surface disturbance.

Test 1 conditions	
β	20°
$p_{c,1}$	63.4 to 59.9 kN/m^2
$p_{c,2}$	65.2 to 59.5 kN/m^2
$p_{c,3}$	63.4 to 56.6 kN/m^2
p_{∞}	0.4 kN/m^2
h/d_e	522 to 38.6
$\overline{v}$	2.53 m/s
$\overline{p}_e/p_{\infty}$	9.3

h/d_e = 522 to 38.6   L-70-1896

Test 4 conditions	
β	20°
$p_{c,1}$	68.7 to 59.3 kN/m^2
$p_{c,2}$	67.3 to 58.5 kN/m^2
$p_{c,3}$	64.1 to 56.3 kN/m^2
p_{∞}	0.4 kN/m^2
h/d_e	528 to 21.9
$\overline{v}$	2.60 m/s
$\overline{p}_e/p_{\infty}$	9.2
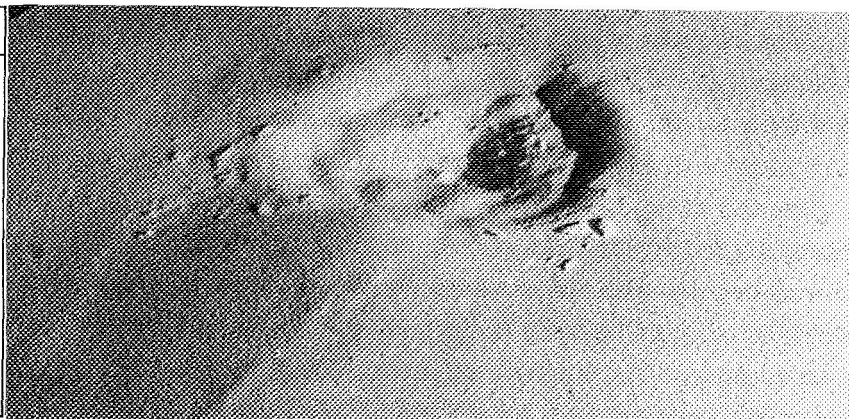
h/d_e = 528 to 21.9   L-70-1939

(b) $\beta = 20^{\circ}$.

Figure 9.- Concluded.

Additional Comments

Spacecraft altitude at start of erosion.- The motion pictures of some of the tests were examined to determine the spacecraft altitude at which the target surface just began to move under the action of the impinging rocket exhaust gases. This altitude was determined to range from about $450d_e$ for the tests at an ambient pressure of 0.8 kN/m^2 to about $350d_e$ for the tests at an ambient pressure of 0.4 kN/m^2. There were insufficient data to ascertain any effect of rocket cant angle on incipient erosion altitude.

Base pressures.- No base pressures were detected during the present tests. A previous investigation of Apollo lunar module base pressures (ref. 7) suggests that the model spacecraft must descend to a much lower altitude before perceiving pressure effects from surface-reflected rocket exhaust gases.

CONCLUDING REMARKS

An exploratory experimental study has been conducted to determine the relative merits of canting the three retrorockets of the Viking lander toward the center line of the spacecraft as a means of reducing rocket-exhaust disturbance of the surface of Mars. Data are presented for several scaled tests in which cold-gas jets were used to simulate the monopropellant rockets of the actual spacecraft and a surface composed of glass beads represented the surface of Mars.

The results of this exploratory study indicate that canting of the retrorockets toward the center line of the spacecraft does reduce the landing-site disturbance from that produced by a lander configuration with downward-directed retrorockets. The site disturbance pattern changes from three distinct craters (one beneath each rocket) for the rockets directed straight down to a single crater centered beneath the spacecraft for the rockets angled toward the center of the spacecraft. In addition, significantly less material was eroded with the rockets canted. Prior to canting the Viking lander retrorockets, it would of course be necessary to weigh the advantages against the attendant loss of thrust due to canting. The altitude of thrust cutoff also significantly affects site disturbance; surface disturbance was increased as the rockets descended closer to the surface before thrust cutoff. In addition, the onset of surface disturbance was found to occur while the model spacecraft was still relatively high above the surface.

Langley Research Center,
National Aeronautics and Space Administration,
Hampton, Va., August 6, 1970.

REFERENCES

1. Viking Project Management: 1973 Viking Voyage to Mars. Astronaut. Aeronaut., vol. 7, no. 11, Nov. 1969, pp. 30-59.

2. Foreman, K. M.: The Interaction of a Retro-Rocket Exhaust Plume With the Martian Environment. Grumman Res. Dep. Mem. RM-354, Grumman Aircraft Eng. Corp., Feb. 1967.

3. Romine, G. L.: Retro Rocket Heating of the Martian Surface. TM 0471/20-10-25-68, Martin Marietta Corp., Oct. 1968.

4. Hutton, Robert E.: Mars Surface Soil Erosion Study. 09349-6001-R000 (JPL Contract No. AX 422060), TRW Systems, Feb. 28, 1968.

5. Thomas, F. W.: Mars Surface Gas Diffusion Study. 09514-6008-R000 (JPL Contract No. 951981), TRW Systems, May 27, 1968.

6. Roberts, Leonard; and South, Jerry C., Jr.: Comments on Exhaust Flow Field and Surface Impingement. AIAA J. (Technical Comments), vol. 2, no. 5, May 1964, pp. 971-974.

7. Clark, Leonard V.: Experimental Investigation of Close-Range Rocket-Exhaust Impingement on Surfaces in a Vacuum. NASA TN D-5895, 1970.

TABLE 1.- CHARACTERISTICS OF VIKING LANDER DESCENT
PROPULSION SYSTEM AND MODEL COLD-GAS JETS

Property	Full-scale value	Model value
d_e, cm	15.2	2.54
F, N	[a]756	[a]19.5
M_e	4.21	2.48
p_c, kN/m^2	481	56.0
p_e, kN/m^2	[b]1.74	[b]3.45
R, $\dfrac{m^2}{s^2 \text{-} {}^oK}$	[c]650	2080
T_c, ^oK	1110	278
T_e, ^oK	[b]304	[b]91
γ	1.30	1.67
ϵ	20	2.11
θ_e, deg	8.3	8.1

[a]For an ambient pressure of 0.4 kN/m^2.

[b]From one-dimensional compressible-flow equations.

[c]For a gas molecular weight of 12.8.

TABLE 2.- SUMMARY OF EXPERIMENTAL TEST CONDITIONS

Test	Ambient pressure, p_∞, kN/m²	Combustion-chamber pressure, $\bar{p}_c$, kN/m²	Rocket cant angle, β, deg	Rocket altitude ratio, h/d_e	Descent velocity, $\bar{v}$, m/s	Pressure ratio, $\bar{p}_e/p_\infty$	Single rocket thrust, $\bar{F}_M$, N
1	0.4	61.3	20	522 to 38.6	2.53	9.3	21.3
2	.4	67.9	0	523 to 21.8	2.61	10.3	23.6
3	.4	60.5	10	525 to 21.8	2.69	9.2	21.0
4	.4	62.3	20	528 to 21.9	2.60	9.2	21.6
5	.8	59.7	0	539 to 21.1	2.63	4.5	20.6
6	.8	71.0	15	535 to 20.9	2.61	5.4	24.6
7	.8	59.4	0	527 to 22.9	1.30	4.5	20.5
8	.8	57.2	10	530 to 22.9	1.29	4.3	19.7
9	.4	58.0	10	534 to 38.6	2.57	8.8	20.1

TABLE 3.- SUMMARY OF EXPERIMENTAL TESTS RESULTS

Test	Description of surface disturbance
1	A single crater centered beneath the model spacecraft with $d = 26.7$ cm and $y = 2.23$ cm. Estimated volume of eroded material was 410 cm^3. (Conical crater was assumed.)
2	A crater beneath each rocket with $\bar{d} = 26.7$ cm and $\bar{y} = 3.43$ cm. The center of the disturbance was 1.42 cm above the original surface. Estimated volume of eroded material was 2950 cm^3.
3	Three overlapping craters beneath the model spacecraft with $\bar{d} = 20.8$ cm and $\bar{y} = 2.79$ cm. The center of the disturbance was 1.75 cm below the original surface.
4	A single crater centered beneath the model spacecraft with $d = 36.1$ cm and $y = 3.35$ cm. Estimated volume of eroded material was 1740 cm^3.
5	A crater beneath each rocket with $\bar{d} = 28.7$ cm and $\bar{y} = 3.45$ cm. Estimated volume of eroded material was 3410 cm^3.
6	A single crater centered beneath the model spacecraft with $d = 44.4$ cm and $y = 4.44$ cm. Estimated volume of eroded material was 3490 cm^3.
7	A crater beneath each rocket with $\bar{d} = 31.0$ cm and $\bar{y} = 2.92$ cm. Estimated volume of eroded material was 3870 cm^3.
8	A single crater centered beneath the model spacecraft with $d = 43.2$ cm and $y = 3.81$ cm. Estimated volume of eroded material was 2840 cm^3.
9	A single crater centered beneath the model spacecraft with $d = 31.8$ cm and $y = 1.42$ cm. Estimated volume of eroded material was 590 cm^3.

"The aeronautical and space activities of the United States shall be
conducted so as to contribute . . . to the expansion of human knowl-
edge of phenomena in the atmosphere and space. The Administration
shall provide for the widest practicable and appropriate dissemination
of information concerning its activities and the results thereof."

— NATIONAL AERONAUTICS AND SPACE ACT OF 1958

NASA SCIENTIFIC AND TECHNICAL PUBLICATIONS

TECHNICAL REPORTS: Scientific and
technical information considered important,
complete, and a lasting contribution to existing
knowledge.

TECHNICAL NOTES: Information less broad
in scope but nevertheless of importance as a
contribution to existing knowledge.

TECHNICAL MEMORANDUMS:
Information receiving limited distribution
because of preliminary data, security classifica-
tion, or other reasons.

CONTRACTOR REPORTS: Scientific and
technical information generated under a NASA
contract or grant and considered an important
contribution to existing knowledge.

TECHNICAL TRANSLATIONS: Information
published in a foreign language considered
to merit NASA distribution in English.

SPECIAL PUBLICATIONS: Information
derived from or of value to NASA activities.
Publications include conference proceedings,
monographs, data compilations, handbooks,
sourcebooks, and special bibliographies.

TECHNOLOGY UTILIZATION
PUBLICATIONS: Information on technology
used by NASA that may be of particular
interest in commercial and other non-aerospace
applications. Publications include Tech Briefs,
Technology Utilization Reports and Notes,
and Technology Surveys.

Details on the availability of these publications may be obtained from:

SCIENTIFIC AND TECHNICAL INFORMATION DIVISION

NATIONAL AERONAUTICS AND SPACE ADMINISTRATION
Washington, D.C. 20546